Vietnam Journal of Earth Sciences, 48(4), 535−560, https://doi.org/10.15625/2615-9783/24715

Vietnam Journal of Earth Sciences
https://vjs.ac.vn/index.php/jse

Late Quaternary sequence stratigraphy and modern sedimentary processes of the northeastern shelf off the Mekong River Delta

Nguyen Trung Thanh[1], Bui Viet Dung[1], Tran Nghi[6], J. Paul Liu[2], Charles A. Nittrouer[3], David J. DeMaster[2], Nguyen Cong Thanh[4,5], Nguyen Kim Dung[1], Hoang Van Long[6], Ngo Thanh Nga[1], Tran Trong Lap[1], An Thi Thuy[1]

[1]*Institute of Earth Sciences, VAST, Hanoi, Vietnam*
[2]*North Carolina State University, USA*
[3]*School of Oceanography, University of Washington, USA*
[4]*Department of Oceanology, Meteorology and Hydrology, University of Science, Ho Chi Minh City, Vietnam*
[5]*Vietnam National University, Ho Chi Minh City, Vietnam*
[6]*Vietnam Geological Association, Hanoi, Vietnam*

Received 13 September 2025; Received in revised form 03 May 2026; Accepted 28 May 2026

ABSTRACT

Research on Late Quaternary sequence stratigraphy of the northeastern shelf off the Mekong River Delta provides critical insights into the evolution of depositional systems in response to global sea-level changes. The integration of sediment stratigraphic frameworks with observations of recent sediment accumulation and transport helps predict the future development of the Mekong River Delta. In this study, seismic and sediment data collected from six cruises (2004−2015) on the inner-middle shelf were processed and interpreted. Two depositional sequences were identified from high-resolution seismic data, designated SQ1 and SQ2. The depositional sequence SQ2 consists of a transgressive systems tract (TST2) and a regressive systems tract (RST2) identified on the middle shelf. The depositional sequence SQ1, overlying SQ2, comprises a transgressive systems tract (TST1) and a highstand systems tract (HST1), developed during the post-LGM transgression after ~19.6 ka. Analysis of SQ1 and SQ2 shows that regressive sediments prevail over transgressive sediments throughout a full fourth-order sea-level cycle (120 ka). Under modern conditions of high relative sea-level rise, spatial variability in sediment accumulation rates from the subaqueous Mekong River Delta to the middle shelf is controlled by hydrodynamic forcing, continental shelf gradient, and variations in sediment transport distance from river mouths: < 2 cm/y on the topset; ~1 to > 10 cm/y on the foreset, with an overall tendency to decrease downslope; < 0.5 cm/y on the bottomset-middle shelf. Sediment accumulation rates are relatively low on the middle shelf. Furthermore, the distribution and characteristics of seabed surface sediments indicate that suspended sediment transport across the middle shelf from west to east along the paleo-Dong Nai River, under the influence of the southwest monsoon, reaches the deep sea. Regulation of sequence stratigraphy and modern sediment processes indicates that the present subaqueous Mekong River Delta has reached the limit of seaward progradation and is gradually shifting to retrogradation.

Keywords: Sea-level change, Late Quaternary, sequence stratigraphy, sediment transport, sediment accumulation rate.

1. Introduction

The northeastern shelf off the Mekong River Delta encompasses the marine areas in front of the Mekong River mouths and the shelf region to the east, northeast off Vung Tau Cape (Fig. 1). This shelf forms part of the broad, gently sloping southeastern

*Corresponding author, Email: thanhtramtich@yahoo.com

Vietnam shelf, which is contiguous with the Sunda Shelf to the south. The study area, with water depths ranging from 0 to 60 m, consists of two distinct coastal zones: (1) the northeastern sector, which is wave-dominated and receives only limited sediment supply from modern small local rivers; and (2) the southeastern sector, which is primarily a deltaic coast shaped by both tidal and wave processes over the past 3,000 years (Ta et al., 2002a) and directly influenced by sediment discharge from the Mekong River, where the subaqueous Mekong River Delta has developed.

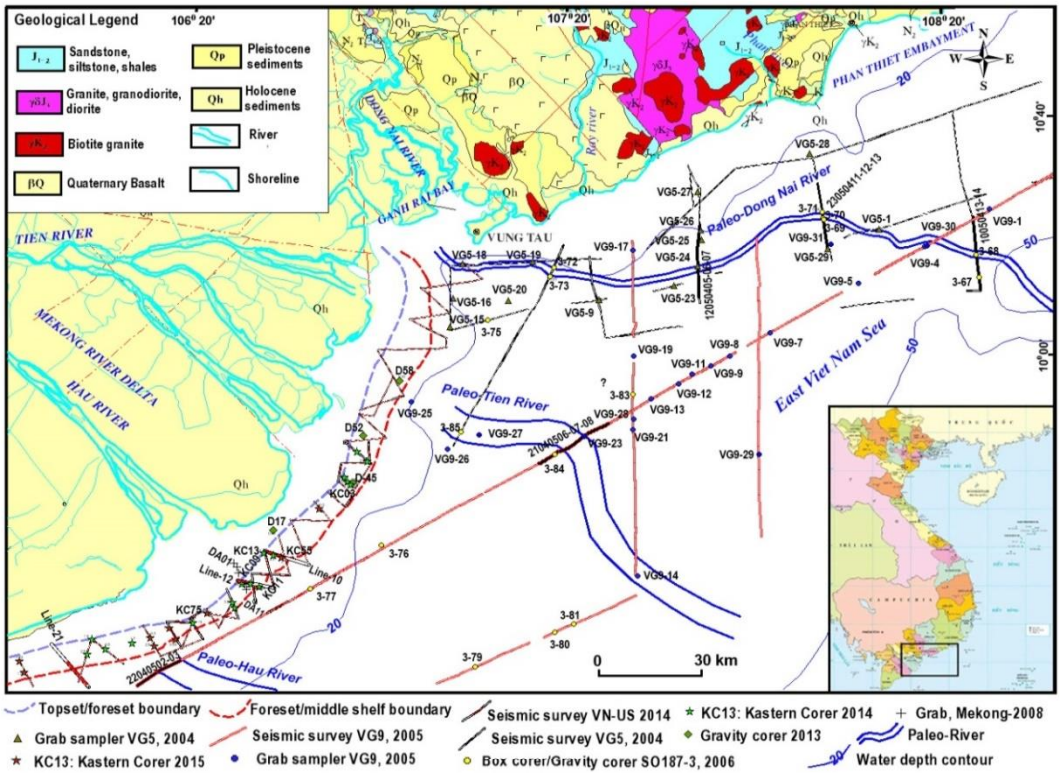

Figure 1. Land geological map of the study area (Quy et al., 2007) with sample locations, and high-resolution seismic profiles from the inner to the middle shelf

In the study area, two major rivers discharge into the sea: the Mekong River and the Sai Gon-Dong Nai River. The Mekong River, one of the 12 longest rivers in the world, with a catchment area of 795,000 km², originates on the Tibetan Plateau and flows through six countries. In Vietnam, the Mekong River splits into two major branches, the Hau and Tien River distributaries. It discharges into the sea through eight mouths (Fig. 1). Before the expansion of large upstream dams in the 1960s, the Mekong delivered a water discharge of 15,000–16,000 m³/s (Milliman and Farnsworth, 2011) and an annual sediment load of 130–160 Mt to the sea (Milliman and Meade, 1983; Milliman and Syvitski, 1992). However, extensive hydroelectric dams and sand mining have reduced the present sediment discharge to about 40 Mt/y (Nowacki et al., 2015). The monsoonal climate strongly controls both river discharge and sediment transport (Wolanski et al., 1996). During the wet season (May-November), stratified saltwater wedges can propagate ~20 km upstream during flood

tides, while ebb-tidal currents dominate and transport sediment seaward to the inner shelf (Nowacki et al., 2015; McLachlan et al., 2017; Eidam et al., 2017). In the dry season (December to April of the following year), salinity intrusion extends up to ~50 km upstream, creating a partially mixed estuary where flood tides dominate and transport suspended sediment landward (Gugliotta et al., 2017, 2018).

Unlike the international Mekong River, the modern Sai Gon-Dong Nai River system discharges into the sea in the northeast of the Mekong River Delta. It is the largest River wholly within Vietnam's territory. The mouths of Sai Gon-Dong Nai River system do not exhibit well-developed subaqueous deltaic features (sediment wedges or clinoforms). The Sai Gon-Dong Nai River system consists of two rivers: the Dong Nai and Sai Gon Rivers. The Dong Nai River basin spans approximately 38,600 km² and has a water discharge of 613 m³/s. In comparison, the Saigon River basin covers around 5,000 km² and has a water discharge of 50 m³/s (Nguyen et al., 2019).

During sea-level lowstands of Marine Isotope Stages (MIS) 6 and 2, both the Dong Nai and Mekong Rivers, also known as paleo-rivers, extended across the continental shelf and reached the shelf break at approximately 120 meters in water depth (Thanh et al., 2021). During subsequent transgressions, incised valleys of these paleo-rivers were infilled. Investigation of the Late Quaternary sequence stratigraphy on the northeastern shelf off the Mekong River Delta provides valuable insights into the sedimentary history of this region. Further, this study refines and further supports the stratigraphic models proposed by Thanh et al. (2021) and Bui et al. (2013). This research contributes to elucidating sedimentary systems tracts over the past 140 ka (calibrated thousand years before present) under the control of global sea-level changes and the paleo-river systems working on the shelf during the LGM. Observations of depositional systems development under sea-level changes provide an additional scientific base for predicting the future evolution of the modern Mekong River Delta.

In addition, numerous studies have examined sediment dynamics on the southeastern Vietnam shelf, ranging from the subaqueous Mekong River Delta to the middle shelf (e.g., Bui et al., 2009; Xue et al., 2012; Eidam et al., 2017; Liu et al., 2017; DeMaster et al., 2017; Thanh et al., 2017). Analyses of bedform geometry, dimension, and distribution on the shelf indicate a prevailing southwestward sediment transport during the northeast monsoon (Bui et al., 2009). Patterns of sediment transport and accumulation further suggest that waves and coastal currents generated by the northeast monsoon play a dominant role in driving southwestward sediment movement, ultimately forming a distal depositional center around the Ca Mau Peninsula (e.g., Xue et al., 2012, 2014; Hein et al., 2013; Liu et al., 2017; Eidam et al., 2017; Thanh et al., 2017). Several studies have focused on sediment accumulation on the subaqueous Mekong River Delta (DeMaster et al., 2017; Eidam et al., 2017; Liu et al., 2017). However, there is little information on sediment accumulation on the northeastern middle shelf off the Mekong River Delta. This data gap hinders a comprehensive understanding of the factors controlling modern sediment accumulation on the middle shelf. Cross-shelf sediment transport has not been reported in previous studies. The integration of modern sedimentary processes and sequence stratigraphy in the study area is crucial for improving predictions of the future of the Mekong River Delta under ongoing global sea-level rise and human activities.

In this study, we integrated published and unpublished high-resolution seismic data and sediment accumulation rates from the subaqueous Mekong River Delta in front of the river mouths to the middle shelf offshore Vung Tau Cape (Fig. 1). We proposed a conceptual combined stratigraphic and sediment-accumulation-regulation model. On the other hand, the distribution patterns of surface sediments were used to identify pathways and trace suspended sediment transport across the shelf under the influence of the southwest monsoon. Finally, the future evolution of the subaqueous Mekong River Delta is predicted.

Objectives of this study:

- To refine the Late Quaternary sequence stratigraphic framework under sea-level changes and reveal the vigorous development of deltaic sedimentation during relative sea-level fall.
- To elucidate recent sediment accumulation and suspended sediment transport across the shelf, supporting the prediction of the future evolution of the subaqueous Mekong River Delta.

2. Background of the research area

2.1. Regional setting

In the northern coastal sector, biotite granite is of upper Cretaceous age. It is distributed along the coast and landward (Quy et al., 2007) (Fig. 1). The biotite granite is exposed in some onshore areas, creating headlands along the coastline. Rhyolite and dacite appear in a small mass near the coast. Quaternary basalt extends from inland to near the modern coast. Quaternary sediments mainly consist of sand and are older landward, with Pleistocene age, while younger sediments seaward are Holocene.

In the southern coastal sector, no volcanic or intrusive rocks are exposed on the land surface. Most of the exposed sediments consist of Holocene deposits (Fig. 1). Onshore investigations indicate that these Holocene sediments were deposited over the last 6.0 ka (Ta et al., 2002a, b; Nguyen et al., 2010). The majority of sediment deposited during the middle to late Holocene belongs to a deltaic facies association (Ta et al., 2002a). The Mekong River Delta represents a typical mixed-energy delta influenced by both tides and waves, with a wide delta plain formed over the past 6.0 ka (Ta et al., 2002a).

The study area is located on the southeastern shelf of Vietnam, which connects southward to the Sunda Shelf within the Southeast Asian continental shelf system. This region belongs to a passive continental margin characterized by low seismicity and weak present-day tectonic deformation (e.g., Morley, 2012; Schmidt et al., 2019). High-resolution seismic studies indicate that Late Quaternary stratigraphic development is primarily controlled by sedimentary processes, with minimal tectonic influence (e.g., Bui et al., 2013; Thanh et al., 2021). Moreover, recent studies demonstrate that modern subsidence in the delta is largely driven by anthropogenic factors, such as groundwater extraction, rather than tectonic activity (Minderhoud et al., 2017, 2018).

The bathymetry of the interested area indicates that the shelf narrows northward, with a steeper gradient than in the southern sector. The subaqueous Mekong River Delta extends to water depths of approximately 20–22 m (Liu et al., 2017). It is distributed south of Vung Tau Cape, occupies the offshore area in front of the Mekong River mouths, and extends toward the Ca Mau Peninsula (Liu et al., 2017; Xue et al., 2010). On the middle shelf, several sand wave fields were observed (Bui et al., 2009).

Hydrodynamic processes in the study area are influenced by a complex interplay of factors, including the monsoonal climate, river discharges, winds, waves, coastal currents, and tides. The region is strongly affected by the Asian tropical monsoon, which

features two opposing seasons: the northeast monsoon or winter monsoon (November to March) and the southwest monsoon or summer monsoon (May to September), with transitional periods in April and October (Matsumoto, 1997). The northeast monsoon almost corresponds with the dry season (December to April), while the southwest monsoon approximately coincides with the wet season (May to November). During the northeast monsoon, prevailing winds and waves predominantly come from the northeast or east; conversely, during the southwest monsoon, they reverse direction, dominating southwestward (Marchesiello et al., 2019). Water level fluctuations along the coast are primarily driven by semi-diurnal tides, with maximum ranges of approximately 3.5 to 4.0 meters at the river mouths (Bui et al., 2009; McLachlan et al., 2017; Nguyen et al., 2023).

2.2. Sea-level changes

Global sea-level changes over the past 500 ka have been extensively studied worldwide (e.g., Rohling et al., 1998; Lambeck & Chappell, 2001; Waelbroeck et al., 2002). Within the last 150 ka, periods of sea-level highstands correspond to Marine Isotope Stages (MIS) 5, and 1, while sea-level lowstands occurred during MIS 6, and 2 (Fig. 2A). During the Late Pleistocene, sea level reached the highest altitude at approximately +6 meters above the present sea level in MIS 5e, between 128 and 116 ka (e.g., Lambeck & Chappell, 2001; Carr et al., 2010; Pan et al., 2018). Following this, sea level declined in an oscillatory pattern, reaching a minimum lowstand of 120±6 meters below present sea level (BPSL) in MIS 2, corresponding to the Last Glacial Maximum (LGM) (Hanebuth et al., 2000, 2009; Clark et al., 2009).

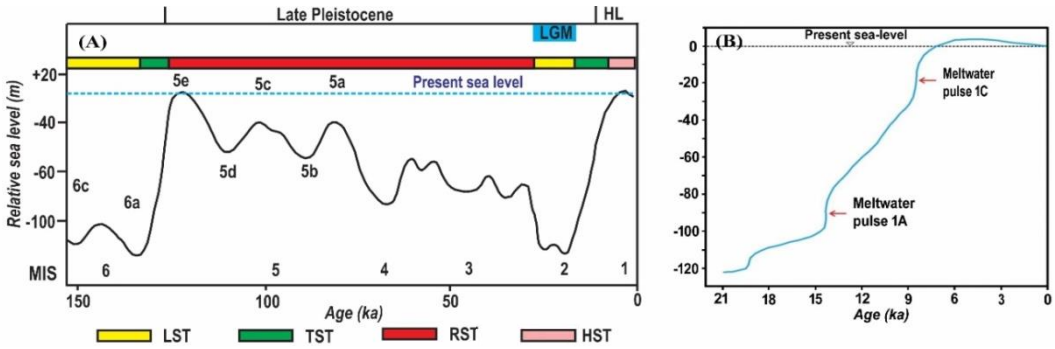

Figure 2. (A) Pacific sea-level change after Waelbroeck et al. (2002) for the past 150 ka and classification of systems tracts based on the sea-level curve (Modified from Thanh et al., 2021); (B) Sea-level changes since the Last Glacial Maximum (LGM) compiled from Tanabe et al. (2006), Hanebuth et al. (2011), Stattegger et al. (2013), and Tjallingii et al. (2014)

The high-resolution sea-level change curve had been reconstructed since the LGM based on the data compiled from Tanabe et al. (2006), Hanebuth et al. (2011), Stattegger et al. (2013), and Tjallingii et al (2014) for the East Vietnam Sea (Fig. 2B) (Thanh et al., 2023; 2026). Three meltwater pulses were identified, including the initial pulse, Meltwater pulse 1A, and Meltwater pulse 1C (Fig. 2B). Meltwater pulse 1B was not clearly identified in this case or in other regions of the world. The initial pulse occurred from 19.6 to 18.6 ka (Hanebuth et al., 2009). Meltwater Pulse 1A took place around 14.6–14.2 ka, followed by Meltwater Pulse 1C around 11.0–8.0 ka. After 8.0 ka, the rate of sea-level rise slowed, eventually reaching a mid-Holocene highstand of +1.5 to +3 meters around 6 ka (Tanabe et al., 2006; Hanebuth et al., 2011; Stattegger et al., 2013; Tjallingii et

al., 2014). Over the past 5.5 ka, sea level gradually fell approximately 2.0–2.5 m (Tanabe et al., 2006; Stattegger et al., 2013). However, the trend of sea-level fall ceased and was replaced by modern sea-level rise at the average rate of 1.7±0.2 millimeters for the past 150 years (Church and White, 2011) and especially a higher rate of 3.6–4.0 millimeters per year in the past 20 years (Hay et al., 2015; Masson-Delmotte et al., 2021).

3. Documents and Methods

3.1. Documents

In this research, we present several unpublished seismic profiles collected during cruises VG5 (2004) and VG9 (2005), the result of collaborations between the University of Kiel and the Institute of Earth Sciences. Additionally, seismic data from the 2014 and 2015 cruises, conducted jointly by the University of Washington, North Carolina State University, and the Institute of Earth Sciences, are incorporated to elucidate the Holocene sequence stratigraphy and sedimentation on the inner to middle continental shelf.

Grain-size analysis data of fifty-one surface sediment samples collected during cruises VG5 (2004), VG9 (2005), SO-187-3 (2006), and Mekong-2008 were used to characterize seabed sediment distribution (Table 1). Gravity-core data, including sediment characteristics and previously published radiocarbon (^{14}C) ages (Tjallingii et al., 2010), were employed to support the interpretation of high-resolution seismic profiles. In addition, some unpublished ^{210}Pb data were processed from sediment cores collected during cruises in 2004 (in collaboration with Kiel University) and in 2013, 2014, and 2015 (in collaboration with the University of Washington and NC State University).

Table 1. Grain-size analysis results of collected surface samples in the study area

No	Sample Name	Coordinates (Degree)	Water depth (m)	Gravel (%)	Sand (%)	Mud (%)	Sediment texture group
1	VG5-01	108.162/10.356	48	0.0	51.2	48.3	Muddy sand
2	VG5-9	107.407/10.164	31.5	0.0	82.0	18.0	Muddy sand
3	VG5-15	107.007/10.092	21.8	0.0	93.9	6.1	Sand
4	VG5-16	107.016/10.171	18.2	0.0	28.83	71.2	Sandy mud
5	VG5-18	107.043/10.267	22	0.0	49.1	50.4	Sandy mud
6	VG5-19	107.232/10.274	23	0.0	73.1	26.9	Muddy sand
7	VG5-20	107.164/10.165	30	0.0	94.4	5.6	Sand
8	VG5-23	107.610/10.204	38	0.0	84.2	15.8	Muddy sand
9	VG5-24	107.623/10.257	31	0.0	80.3	15.6	Muddy sand
10	VG5-25	107.684/10.331	25	0.0	92.2	7.8	Sand
11	VG5-26	107.683/10.357	23.3	0.0	96.5	3.5	Sand
12	VG5-27	107.675/10.465	18.4	0.2	97.1	2.7	Slightly gravelly sand
13	VG5-28	107.978/10.569	26.4	0.0	94.8	5.2	Sand
14	VG5-29	108.025/10.301	52	0.0	85.2	14.8	Muddy sand
15	VG9-1	108.458/10.408	49	0.0	96.1	3.8	Sand
16	VG9-4	108.282/10.305	49	0.0	44.5	55.5	Sandy mud
17	VG9-5	108.104/10.204	45	0.3	67.4	32.4	Muddy sand
18	VG9-7	107.866/10.068	38	6.0	76.1	17.9	Gravelly muddy sand
19	VG9-8	107.758/10.005	35	2.5	90.8	6.7	Sand
20	VG9-9	107.707/9.979	33	0.0	96.2	3.8	Sand
21	VG9-11	107.656/9.955	34	0.6	92.1	7.3	Sand
22	VG9-12	107.620/9.928	33	3.5	89.8	6.7	Slightly gravelly sand
23	VG9-13	107.545/9.886	30	1.4	95.3	3.3	Slightly gravelly sand
24	VG9-14	107.506/9.392	33	9.2	85.9	4.9	Gravelly sand
25	VG9-17	107.500/10.302	22	0.1	83.8	16.1	Muddy sand

No	Sample Name	Coordinates (Degree)	Water depth (m)	Gravel (%)	Sand (%)	Mud (%)	Sediment texture group
26	VG9-19	107.499/10.008	30	3.4	89.0	7.5	Slightly gravelly, muddy sand
27	VG9-21	107.497/9.801	34	20.6	73.8	5.0	Gravelly sand
28	VG9-23	107.366/9.783	29	0.1	97.2	2.8	Sand
29	VG9-25	106.901/9.883	21	0.0	68.5	31.5	Muddy sand
30	VG9-26	106.999/9.750	22.5	0.0	95.8	4.2	Sand
31	VG9-27	107.083/9.789	29.2	0.2	97.1	2.7	Slightly gravelly sand
32	VG9-28	107.499/9.829	33.5	0.1	96.8	3.1	Sand
33	VG9-29	108.834/9.730	44	3.8	82.9	6.9	Slightly gravelly sand
34	VG9-30	108.291/10.308	50	0.0	37.3	62.7	Sandy mud
35	VG9-31	108.032/10.315	55	0.0	23.7	76.3	Sandy mud
36	187-3-67	108.429/10.219	56	1.8	83.2	15.0	Slightly Gravelly muddy sand
37	187-3-70	108.012/10.388	41.5	0.0	79.3	20.7	Muddy sand
38	187-3-71	108.010/10.405	38	4.1	87.4	8.6	Slightly gravelly sand
39	187-3-72	107.288/10.256	26	0.0	89.5	10.5	Muddy sand
40	187-3-75	107.110/10.110	21	0.4	96.9	2.7	Slightly gravelly sand
41	187-3-76	106.819/9.483	24	1.7	93.4	4.9	Sand
42	187-3-79	107.069/9.141	33	0.7	96.8	2.5	Slightly gravelly sand
43	187-3-80	107.283/9.235	38	11.0	86.0	2.9	Gravelly sand
44	187-3-81	107.333/9.258	38	2.5	94.8	2.7	Slightly gravelly sand
45	187-3-83	107.497/9.899	31	2.4	94.1	3.5	Slightly gravelly sand
46	187-3-85	107.035/9.797	27	0.0	97.2	2.8	Sand
47	DA01	106.425/9.434	4	0.0	97.3	2.7	Sand
48	DA02	106.434/9.422	4	0.0	100	0.0	Sand
49	DA04	106.438/9.406	4	0.0	99.0	1.0	Sand
50	DA08	106.453/9.374	12	0.0	17.1	82.9	Sandy mud
51	DA11	106.457/9.359	15	0.0	14.6	85.4	Sandy mud

3.2. Methodology

3.2.1. Seismic acquisition and interpretation

High-resolution seismic data were acquired using a Boomer and a Chirp-sonar profiler as acoustic sources during the surveys. Because the focus of this research was the inner-middle shelf, the seismic profiles were located mostly at water depths of 5–60 m. The vessel's average speed was 4 kn during the surveying period. The Boomer system is a single-channel system that includes an electrical energy supply and an electromagnetic transducer that converts the discharged energy into electrodynamic acoustic pulses. The boomer source produces a wide bandwidth, with a main range of 0.3 to 11 kHz. This wide bandwidth results in a typical penetration depth of 20 to 100 m below the seabed, depending on the nature of the sub-seafloor strata.

On the other hand, the Chirp sonar profiler operates in the 0.5–12 kHz frequency range, allowing it to penetrate up to 10 meters into the seabed. The system typically consists of a transducer that emits sound pulses, a receiver that detects the reflected signals, and a processing unit that interprets the data to generate images of the subsurface layers. The sound waves emitted by both the Boomer and Chirp sonar profilers travel through the water column and into the seabed, where they are reflected back at interfaces between different sediment or rock layers. These are known as acoustic impedance contrast boundaries. By analyzing the travel time of the returning sound waves, the system can determine the depth and thickness of these layers and detect geological features. Seismic data were processed and interpreted using NWC and Reflexw software. The depth was calculated with the assumption that the acoustic wave

velocity is 1500 m/s in water and 1600 m/s in seabed sediments.

Several authors have proposed classifications of systems tracts and sequence-stratigraphic surfaces based on various case studies (e.g., Vail, 1987; Van Wagoner et al., 1988; Posamentier and Allen, 1999). Catuneanu et al. (2011) summarized and standardized the classification scheme, including four systems tracts: highstand systems tract (HST), falling stage systems tract (FSST), lowstand systems tract (LST), and transgressive systems tract (TST). In this research, we examine two sequences for the past 140 ka. For the youngest sequence (SQ1), we can determine the depositional systems tracts TST1 and HST1. However, for the previous sequence (SQ2), separating FSST2 and HST2 is difficult, so we combine HST2 and FSST2 into the regression system tract (RST2). The sedimentary systems tracts were classified on the sea-level curve for the past 140 ka (Fig. 2A). The detailed transgressive systems tract (TST1) in SQ1 follows the pattern of sea-level change since the Last Glacial Maximum (LGM) (Fig. 2B).

3.2.2. Grain size analysis

Grain-size analysis of surface sediment samples (collected from 0–5 cm on the seabed) was performed using a sieving system with mesh sizes of 62.5 µm, 125 µm, 250 µm, 500 µm, 750 µm, 1000 µm, and 2000 µm. Fine sediment samples were additionally analyzed using a Mastersizer 2000 laser diffraction system. Sediment samples were first dried at 60°C for 24 hours, after which approximately 50–70 g of each sample was weighed and sieved. The weight of sediments retained on each sieve was recorded, and the proportion of each size fraction was calculated relative to the total sample weight. Grain-size parameters were subsequently derived. In this study, we report the proportions of gravel, sand, and mud. A ternary diagram based on the percentages of mud, sand, and gravel was used to classify surface sediment textures (Folk, 1954). Grain-size analyses of samples were conducted at the University of Kiel and the Institute of Earth Sciences in Vietnam in 2004–2008.

3.2.3. Measurement of ^{210}Pb radioactivity

The ^{210}Pb activities were measured using the ^{210}Po method, as secular equilibrium between the two isotopes had been verified and the extraction and measurement of ^{210}Po is favorable. The sediment samples were dried, and 5–10 g of each sample were spiked with a known amount of artificial ^{208}Pb for yield determination. The dried samples were digested with a mixture of HNO_3 and $HClO_4$, then with HCl. The final residue was diluted with HCl, and the solution was separated from particulates by centrifugation. The isotopes ^{208}Po and ^{210}Pb were then extracted from the solution by spontaneous electrodeposition onto silver discs. The alpha decays from both isotopes were measured using a silicon surface-barrier detector connected to a pulse-height analyzer. In this research, sediment cores were analyzed in the laboratories of the University of Washington and NC State University, USA, in 2013, 2014, and 2015. Sediment accumulation rates were calculated for this research.

3.2.4. Calculating the sediment accumulation rate

Linear sediment accumulation rate (SAR) was determined from the exponential downcore decline in excess ^{210}Pb activity below the surface layer, assuming a constant initial radionuclide concentration (despite variable sediment accumulation rates) using the equation of Robbins and Edgington (1975) and McKee et al. (1983).

$$SAR = \lambda \times z \times [Ln(A_0/A_z)]^{-1} \quad (1)$$

Where z is the depth in the core (cm), A_0 is the specific activity of excess ^{210}Pb at a particular reference horizon (dpm/g), normally coinciding with the surface layer of the core, and A_z is the specific activity of excess ^{210}Pb at depth z below the reference horizon (dpm/g), λ is the decay constant and has a value of 0.0311.

4. Results

4.1. Late Quaternary Stratigraphy

4.1.1. Sequence stratigraphy surfaces

Two sequence boundaries (SB1 and SB2) were recognized, and the surfaces TS1, TRS1, MFS1, and MFS2 were also identified on the seismic profiles in this research.

SB1 is characterized by highly continuous, strong-amplitude reflections across all seismic profiles (Figs. 3–8). This surface can be traced across the shelf in water depths ranging from 20 to 60 meters. However, in shallower areas closer to shore (0–20 m water depth), shallow gas effects obscure reflections, preventing the identification of SB1 in these zones.

TS1 is a surface that occurs within incised-valley systems, characterized by moderate-amplitude, continuous reflections in seismic profiles (Figs. 3–5 and 7). In the upper edge of the incised-valley systems, it is almost merged with the lower SB1 surface and upper TRS1 surface.

TRS1 is a surface that was determined from sediment cores and seismic profiles (Figs. 3–8) mostly within incised valleys and adjacent areas. It is characterized by moderate-amplitude, continuous reflections in the seismic profiles. It merges with SB1 and TS1 at the edges of incised valleys.

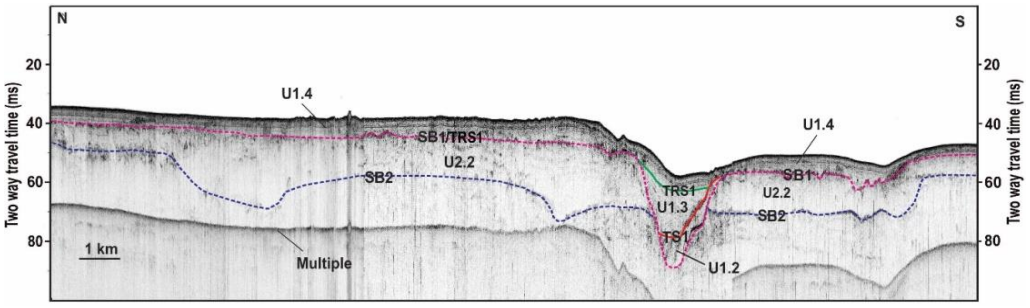

Figure 3. Profile 12050405-06-07 showing SB2, SB1, TS1 and TRS1 surfaces, and sedimentary units U2.2, U1.2, U1.3, and U1.4; incised valley of paleo-Dong Nai River

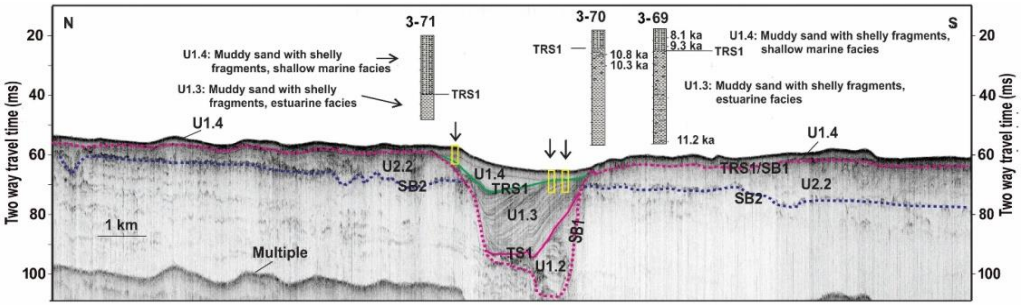

Figure 4. Profile 23050411-12-13 showing SB2, SB1, TS1, and TRS1 surfaces; seismic units U2.2, U1.2, U1.3, and U1.4; incised valley of paleo-Dong Nai River

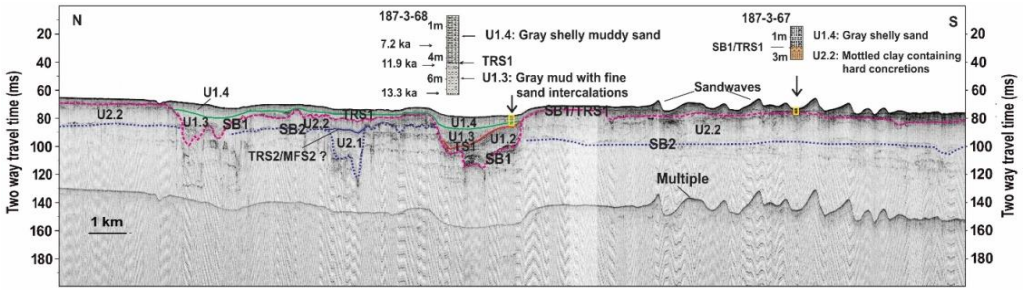

Figure 5. Profile 10050413-14 showing SB2, SB1, TS1, TRS1 surfaces; seismic units U2.1, U2.2, U1.2, U1.3, and U1.4; incised valleys of paleo-Dong Nai River; and sand waves (Modified from Thanh et al., 2021; Bui et al., 2013)

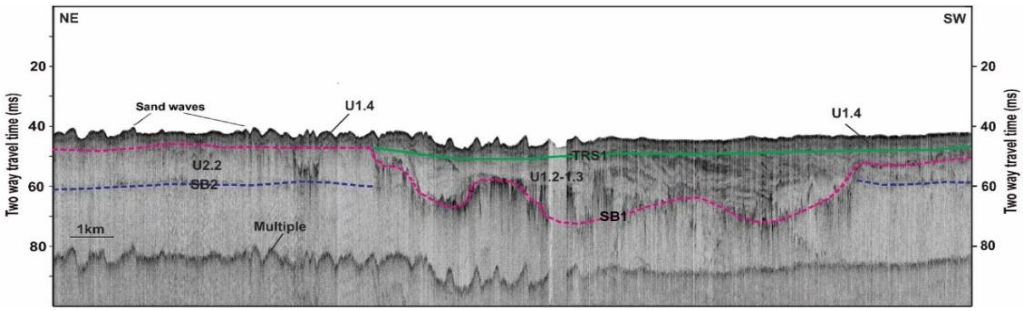

Figure 6. Profile 21040506-07-08 showing SB2, SB1, and TRS1 surfaces; U2.2; U1.2-1.3; U1.4; incised valley of paleo-Tien River (a major branch of paleo-Mekong River), and sand waves

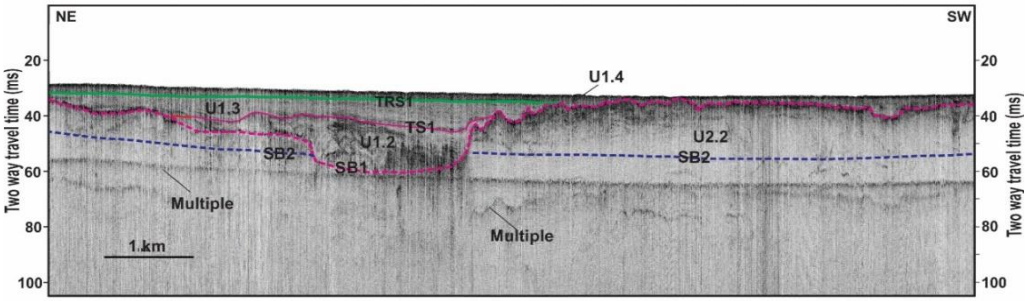

Figure 7. Profile 22040502-03 shows SB2, SB1, TS1, and TRS1 surfaces, U2.2, U1.2, U1.3, and U1.4; incised valley of paleo-Hau River (a major branch of paleo-Mekong River)

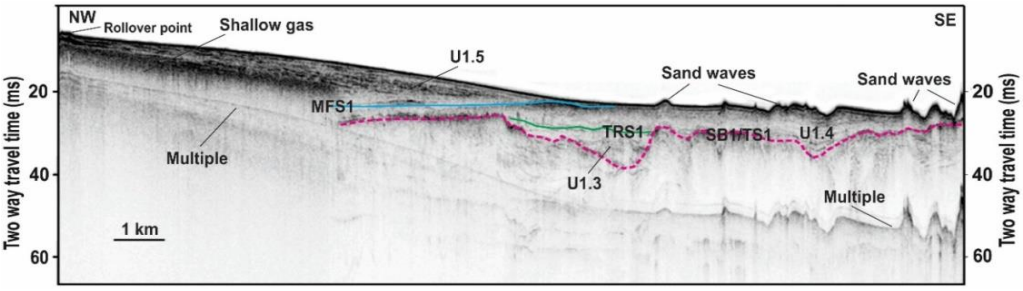

Figure 8. Profile Line-21 shows SB1, TRS1, and MFS1 surfaces; and seismic units U1.3, U1.4, and U1.5; and sand waves on the seabed

MFS1 is a surface identified on the inner shelf around the modern Mekong subaqueous delta (0–22 m depth). It is clearly observed on seismic profiles as a high-amplitude, continuous surface that marks the boundary between a lower, sheet-like, transparent reflector unit and an overlying unit characterized by seaward-dipping reflectors (Fig. 8).

SB2 is an obvious surface, low amplitude, low continuity that is underlying the SB1, and is usually identified adjacent to areas of incised valleys (Figs. 3–7).

MFS2 is characterized by low-amplitude and low-continuity reflections and is identified in several older incised valleys beneath the SB1 surface (Fig. 5), separating U2.1 from U2.2.

4.1.2. Depositional sequence SQ1

In this research, we focused on the inner-middle shelf to elucidate sedimentary structures along paleorivers. Four sedimentary units were identified on the shelf within depositional sequence SQ1, including U1.2, U1.3, U1.4, and U1.5. The unit U1.1, as the lowstand wedge on the shelf break, was proposed in the previous studies (Bui et al., 2013; Thanh et al., 2021).

Unit U1.2 was identified as the basal part or as a lateral unit within incised valleys. The seismic facies is characterized by strong reflectivity and weakly developed, chaotic layering (Figs. 3–5 and 7). This unit directly overlies SB1, as shown in the seismic profiles. U1.2 can be recognized in incised valleys along the paleo-Dong Nai River and within the paleo-Hau River (Figs. 3–5, and 7). In some cases, identifying U1.2 is challenging due to poor seismic data quality and geological complexity. In particular, within some large, incised valleys, U1.2 cannot always be clearly distinguished from the overlying unit U1.3. Therefore, these two units are sometimes combined into a composite unit U1.2–1.3 (Fig. 6).

Unit U1.3 was identified within incised valleys and is characterized by well-defined, continuous layering. In some seismic profiles, however, its internal structure cannot be clearly resolved due to limited seismic resolution, making it difficult to distinguish from the underlying unit U1.2. Unit U1.3 is clearly observed along the paleo-Dong Nai River. The paleo-Hau River (Figs. 3–5, 7) and directly overlies SB1 (Fig. 8). Sedimentary characteristics described by Tjallingii et al. (2010) and Thanh et al. (2021) indicate that U1.3 represents estuarine facies. Core data further constrain its depositional age, ranging from 13.6 to 7.7 ka, with progressively younger ages landward (Tjallingii et al., 2010; Fig. 9).

Unit U1.4 was identified across the entire shelf and represents the Holocene sediment cover. A homogeneous, transparent seismic facies characterizes it. This unit overlies the composite surface SB1/TRS1 on the open shelf and either U1.3 or the composite unit U1.2–U1.3 within the incised valleys (Figs. 3–8). In many areas, seismic profiles show that U1.4 forms sand waves on the seabed (Figs. 3–6, and 8). Sedimentary characteristics described by Tjallingii et al. (2010) and Thanh et al. (2021) indicate that U1.4 corresponds to shallow-marine facies. Core data further constrain its depositional age, ranging from 9.3 to 7.2 ka, with a general trend of progressively younger ages toward the landward margin (Tjallingii et al., 2010; Fig. 9).

Unit U1.5 was identified on the inner shelf at water depths of 0–22 m and represents the modern subaqueous Mekong River Delta. It is characterized by a sedimentary wedge with clinoform structures that taper and pinch out toward the middle shelf at water depths of approximately 20–22 m. The subaqueous Mekong River Delta is the youngest part of the Mekong River Delta and has developed during the last ~3 ka (Xue et al., 2012; Liu et al., 2017). Most of the sediments in U1.5 consist of sandy mud and mud (Eidam et al., 2017; DeMaster et al., 2017; Liu et al., 2017;

Thanh et al., 2017), while some patches of well-sorted fine sand have been identified on the topset of the delta in front of the Hau River mouths (Thanh et al., 2017).

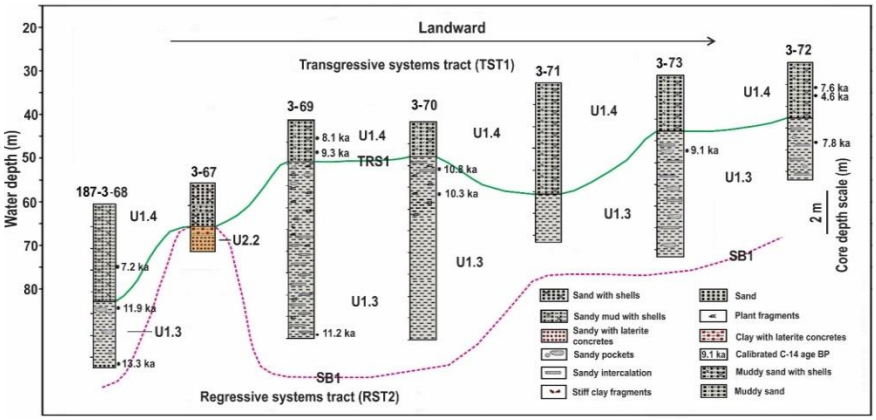

Figure 9. Correlation of sediment cores along the paleo-Dong Nai River offshore Vung Tau Cape (^{14}C dating referenced from Tjallingii et al., 2010)

4.1.3. Depositional sequence SQ2

Sequence SQ2 lies beneath SQ1 and overlies the SB2 surface. It comprises two main units: U2.1 and U2.2. Unlike SQ1, the internal structure of SQ2 is less clearly observed on seismic profiles, primarily because it is an older, deeper sequence with weaker, less continuous reflections.

U2.1 consists of incised-valley fill sediments deposited within an older generation of incised valleys and has a thickness of 8–10 m (Fig. 5).

Unit U2.2 is characterized by relatively homogeneous seismic facies with unclear stratification (Figs. 3-7). It overlies the SB2 surface in areas without incised valleys and overlies U2.1 within the incised valleys. U2.2 has an average sediment thickness of 12–15 m. It was identified in numerous seismic profiles across the shelf, particularly in regions adjacent to the incised valleys of the paleo-Dong Nai River and paleo-Hau River. The thickness of U2.2 is greater than that of U1.4, which directly overlies U2.2 across a large area of the shelf.

4.1.4. Characteristics of incised valleys in SQ1

In a previous study (Thanh et al., 2021), the paleo-river traces across the shelf during the LGM were examined. Studies of incised-valley geometry were also suggested (Bui et al., 2013; Thanh et al., 2021). However, the depth of the incised valleys remains poorly constrained, despite being a key indicator of the shelf-slope gradient. In this study, the dimensions of incised valleys were described in more detail, including their width and depth. Incised valleys of the paleo-Dong Nai River typically range from 2 to 3 km in width and 25–28 m in depth (Figs. 3–5). In contrast, incised valleys associated with the paleo-Tien River and paleo-Hau River are wider and shallower, measuring approximately 7–10 km in width and 18–20 m in depth (Figs. 6 and 7). Based on these morphological characteristics, as well as their spatial distribution and orientation across the shelf, the paleo-river channels can be correlated and traced, allowing for the reconstruction and identification of the individual paleo-channels of each river system (Fig. 1; Thanh et al., 2021).

The paleo-Dong Nai River, which extends eastward across the shelf offshore of Vung Tau Cape, can be regarded as a boundary separating the gently sloping, wide Mekong shelf to the south from the narrower, steeper shelf to the north (Fig. 1). The middle shelf,

north of the paleo-Dong Nai River, is generally elevated. The middle shelf area south of the paleo-Dong Nai is comparatively lower. A distinct narrow depression (2–3 km in width) along the paleo-Dong Nai River can be recognized across the shelf through seismic profiles. The paleo-Dong Nai River flowed along a steeper gradient slope, while the paleo-Hau and paleo-Tien Rivers (major branches of the paleo-Mekong River) flowed across a gentler slope during the LGM. Consequently, incised valleys of the paleo-Dong Nai River are narrower but deeper than those of the paleo-Mekong River system.

4.2. Surface sediment characteristics

The surface sediment texture group includes slightly gravelly sand (sGS), gravelly sand (GS), sand (S), muddy sand (MS), and sandy mud (SM). On the subaqueous delta (inner shelf), sandy mud predominantly covers the seabed. On the middle shelf, the textures comprise slightly gravelly sand (sGS), gravelly sand (GS), sand (S), and muddy sand (SM). Among these, slightly gravelly sand (sGS), gravelly sand (GS), and sand (S) are widely distributed across the shelf. In contrast, muddy sand (SM) and sandy mud (SM) occur mainly along a corridor following the paleo-Dong Nai River.

On the slope of the subaqueous Mekong River Delta (foreset), samples are predominantly sandy mud with mud contents exceeding 80% (Eidam et al., 2017; Thanh et al., 2017). The subaqueous Mekong River Delta serves as the primary depocenter of sandy mud and mud discharged from the Mekong River. On the middle shelf, grain-size analyses indicate sandy textures. However, along the paleo-Dong Nai River, mud content is higher than in the northern and southern parts of the middle shelf (Fig. 10; Table 1). Consequently, surface sediments along the paleo-Dong Nai River exhibit higher mud content (Fig. 10; Table 1).

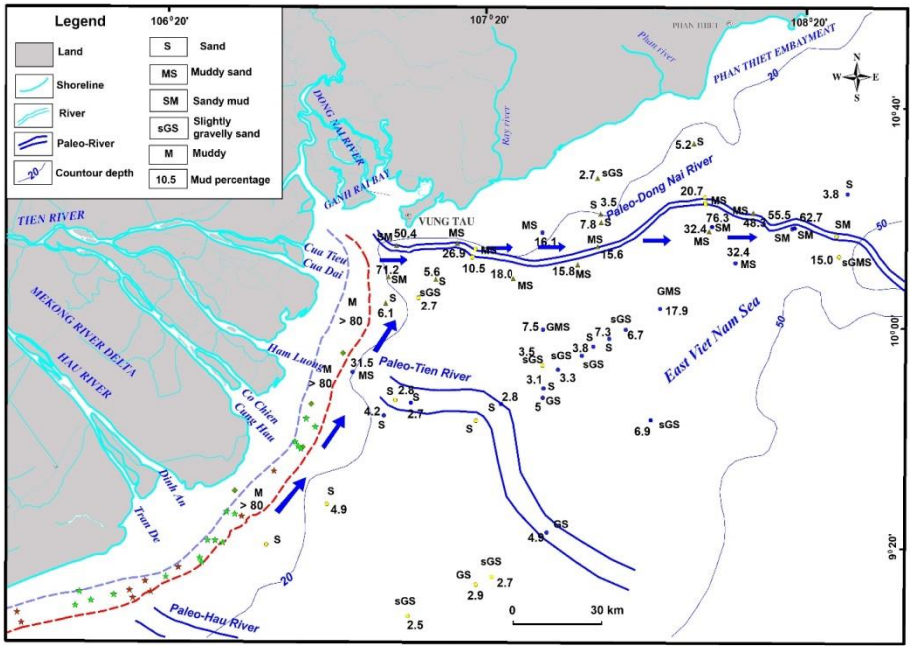

Figure 10. Surface sediment texture group and mud percentage on the northeast shelf off the Mekong River Delta; the blue arrows show the suspended sediment transport across the shelf under the southwest monsoon

4.3. Recent sediment accumulation rates

Most recent estimates of sediment accumulation rates have been derived from the subaqueous Mekong River Delta. In this study, we present unpublished results of recent accumulation rates calculated on three sediment cores collected from the shelf offshore Vung Tau Cape, outside the subaqueous delta. These cores were obtained in 2005 and 2006 along the paleo-Dong Nai River. The analysis of ^{210}Pb in sediments along the paleo-Dong Nai River is feasible because these deposits contain a substantial proportion of mud supplied by suspended sediments, which can adsorb the radionuclide ^{210}Pb from the water column. In contrast, the middle shelf associated with the paleo-Tien and paleo-Hau rivers is dominated by sandy sediments with only minor mud content (less than 5%), making them unsuitable for ^{210}Pb activity measurements. In addition, ^{210}Pb excess activity data from around the Hau River mouths were used to estimate sediment accumulation rates on the inner shelf. Combined with sequence stratigraphy and sediment distribution patterns, these results provide new insight into recent sedimentary processes on the shelf.

The sediment accumulation rates of three cores, VG5-18, SO187-3-73, and SO187-3-71, show the values 0.39 cm/y, 0.09 cm/y, and 0.24 cm/y, respectively, reflecting very low sediment accumulation rates on the middle shelf (Fig. 11). Whereas the subaqueous Mekong River Delta has much higher sediment accumulation rates (Xue et al., 2010; Unverricht et al., 2013; Eidam et al., 2017; DeMaster et al., 2017). In the subaqueous Mekong River Delta, several sediment cores were selected to show a clear sediment accumulation trend on the subaqueous Mekong River Delta from topset (0–5 m in water depth), foreset (5–20 m in water depth), to bottomset-middle shelf (deeper than 20 m). In the Mekong River Delta, the bottomset is very limited and poorly developed compared to other deltas, such as the Mississippi River Delta, the Yangtze River Delta, the Amazon River Delta, the Ganges-Brahmaputra River Delta, the Indus River Delta, and the Gulf of Papua.

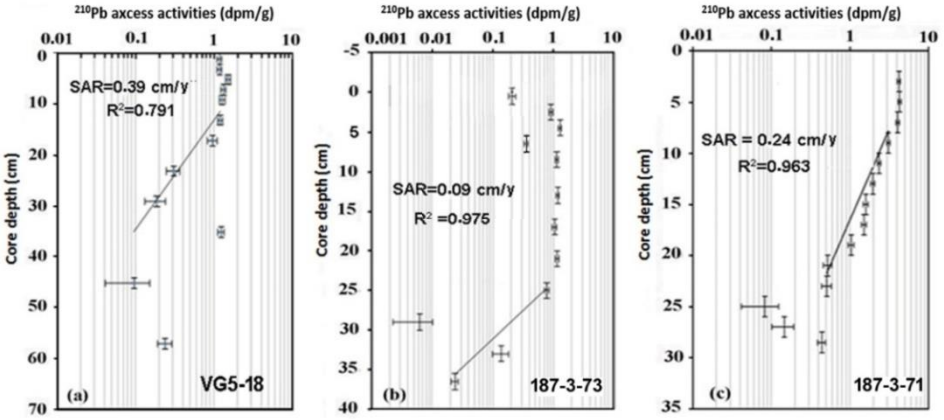

Figure 11. Sediment accumulation rates of three sediment cores: VG-18, 187-73, and 187-71

In this research, one core D17 was collected on the topset at a water depth of 4 m near the shoreline (Fig. 1). The calculated result of sediment accumulation rate is 0.51 cm/y (Fig. 12). Two other cores KC13; KC18 were taken at the rollover of the subaqueous delta at water depth 5–6 m, showing sediment accumulation rates of 2.3 cm/y and 1.8 cm/y (DeMaster et al., 2017, see Table 2). On the foreset, sediment

accumulation rates tend to decrease downward the delta slope: 2.3 cm/y at core KC13 and 1.75 cm/y at core KC55 (Figs. 12 and 15); > 10 cm at core KC03, 3.11 cm/y at core KC04, and 1.95 cm/y at core D45 (Fig. 13); 4.3 cm/y at core KC09; 8.02 cm/y at core KC10; 0.45 cm/y at core KC11 (Figs. 14 and 16).

Overall, the topset generally shows sediment accumulation rates of < 2 cm/y. On the foreset, accumulation rates are higher, ranging from 1 to > 10 cm/y, with a clear downslope decrease (Figs. 12, 13, and 14). Sediment cores collected at the edge of the subaqueous delta, considered the bottomset, record accumulation rates of 0.45 cm/y at core KC11 (Fig. 14), 0.58 cm/y at core KC73 (DeMaster et al., 2017), 0.41 cm/y at core D58 (Table 2), and 0.36 cm/y at core D65 (Table 2). Therefore, the sediment accumulation pattern on the northeastern shelf off the Mekong River Delta can be divided into three zones: (i) topset (< 2 cm/y), (ii) foreset (1– >10 cm/y, with an overall tendency to decrease downslope of the foreset), and (iii) bottomset-middle shelf (< 0.5 cm/y).

These results demonstrate that the northeastern middle shelf off the Mekong River Delta exhibits relatively low accumulation rates. Sequence stratigraphic analysis shows that U1.4 represents the Holocene sediment cover and is mainly composed of sand forming many sand waves on the seabed (Bui et al., 2009).

Table 2. Collected sediment cores and sedimentary environments in the study area

No	Core Name	Core length (cm)	Coordinate (degree)	Water depth (m)	Sedimentary environment	Sediment accumulation rates (cm/y)
1	D17	55	106.530/9.529	4	Delta topset	0.51
2	D45	55	106.715/ 9.632	12	Delta foreset	1.95
3	D52	60	106.772/ 9.787	12	Delta foreset	2
4	D58	50	106.872/ 9.941	17	Delta foreset	0.41
5	KC03	270	106.730/9.660	10	Delta, foreset	>10
6	KC04	290	106.738/9.652	15	Delta foreset	3.11
7	KC09	295	106.445/9.376	7	Delta foreset	4.3
8	KC10	310	106.469/9.375	12.7	Delta foreset	8.02
9	KC11	50	106.492/9.368	19.8	Bottomset-middle shelf	0.45
10	KC13	150	106.505/9.462	6.0	Delta foreset	2.3
11	KC55	170	106.551/ 9.449	17	Delta foreset	1.75
12	VG5-18	60	107.043/10.266	25	Middle shelf	0.39
13	187-3-71	35	108.009/10.404	37	Middle shelf	0.24
14	187-3-73	38	107.278/10.231	31	Middle shelf	0.09

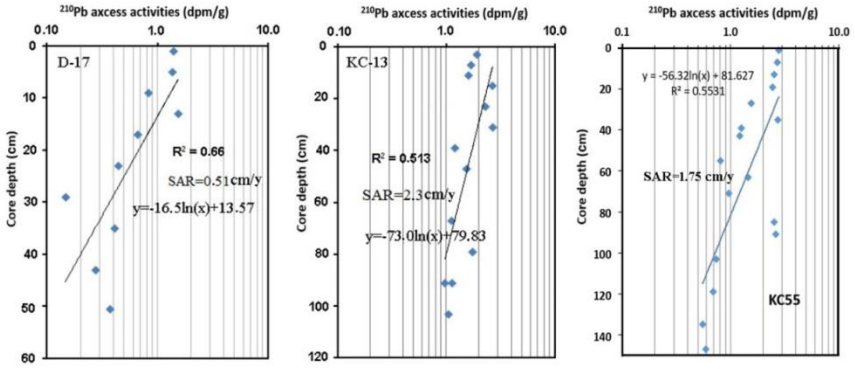

Figure 12. Sediment accumulation rates of cores D-17, KC-13, and KC55

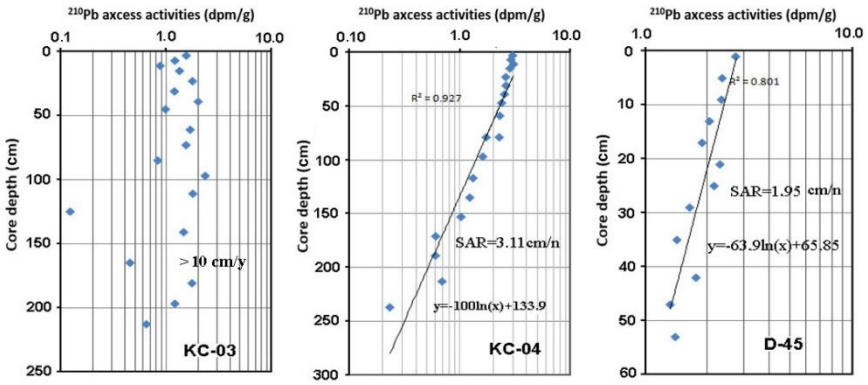

Figure 13. Sediment accumulation rates of three sediment cores: KC03, KC04, and D45

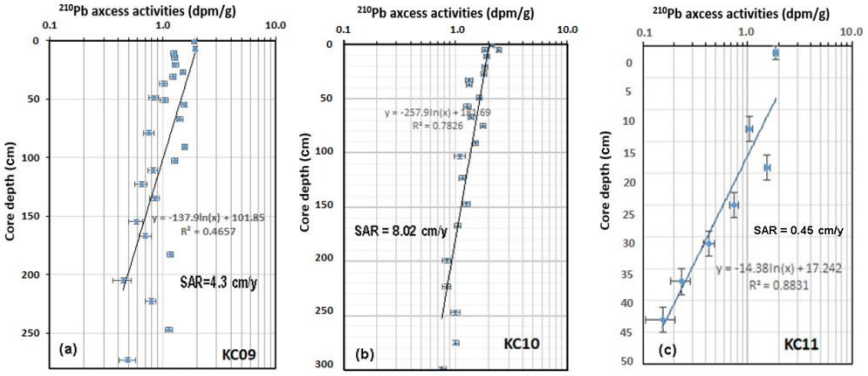

Figure 14. Sediment accumulation rates of three sediment cores: KC09, KC10, and KC11

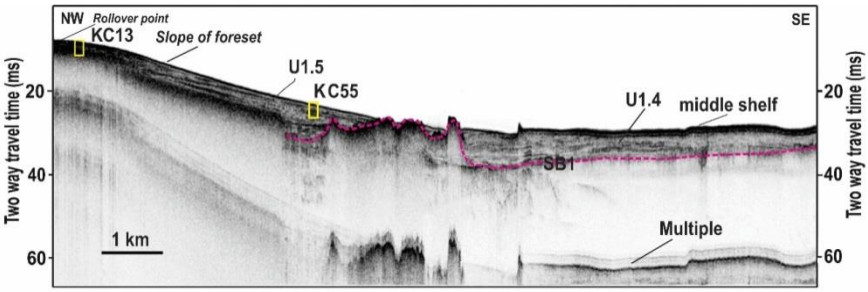

Figure 15. Profile Line-10 showing sediment units U1.4, U1.5, MFS1, surface SB1, and locations of cores KC13 and KC55

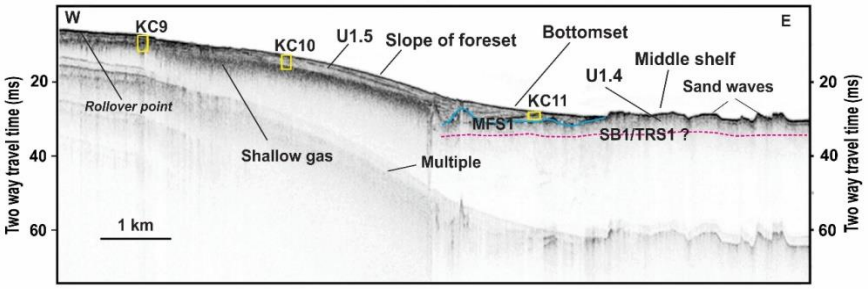

Figure 16. Profile Line-12 (Modified from Eidam et al., 2017, and Liu et al., 2017) showing sediment units U1.4, U1.5, MFS1, sand waves, and locations of cores KC09, KC10, and KC11

5. Discussions

5.1. Sequence stratigraphy

As is well known, sea-level fluctuations during the Quaternary included both lowstands and highstands. Between these two extremes, sea-level rise from a lowstand to the following highstand is referred to as a transgression. In contrast, sea-level fall from a highstand (e.g., MIS 5) to the next lowstand (e.g., MIS 2) is referred to as a regression (Fig. 2A). In this study, we focus on the Late Quaternary (~140 ka), specifically from MIS 6, which corresponds to a lowstand with sea level approximately 120 m below the present level, to MIS 1, the present highstand. Within this interval, one complete sea-level cycle occurred from MIS 6 to MIS 2 (~120 ka), followed by a half cycle from MIS 2 to MIS 1 (~20 ka).

The incised valleys of SQ2 (Fig. 5) were formed during the sea-level lowstand of MIS 6. Subsequent sea-level rise from MIS 6 to MIS 5e led to the infilling of these valleys with sediments (Thanh et al., 2021), resulting in the development of unit U2.1 (Fig. 5). Thus, U2.1 is assigned as the transgressive systems tract (TST2). Since MIS 5e, a prolonged regression (Fig. 4) began ~100 ka ago. During this period, the paleo-Mekong River and paleo-Dong Nai River delivered large volumes of sediment to the shelf. Deltaic sedimentation dominated and extended to the shelf edge (120–150 m water depth) during the sea-level fall. As the sea level fell, these sediments became progressively subaerially exposed and underwent intense weathering under the tropical climate characterized by high humidity and near-equatorial heat. This weathering produced stiff soils that became enriched in iron and aluminum oxides (Thanh et al., 2021). In combination with vegetation growth, which stabilized the land surface, these processes reduced the erosion of deltaic sediments (Thanh et al., 2021). Consequently, during this long regression, the interaction of subaerial exposure and tropical weathering led to the formation of unit U2.2, which became the dominant component of SQ2. U2.2 is clearly observed in numerous seismic profiles on the northeastern shelf off the Mekong River Delta (Figs. 4−7).

Incised valleys of SQ1 were developed during the sea-level lowstand of MIS 2, corresponding to the LGM, forming the sequence boundary SB1. During this period, the major paleo-rivers extended to the shelf break and incised into the underlying sedimentary unit U2.2, as clearly observed in numerous seismic profiles across the shelf (Figs. 3−7). All sediment cores with AMS-^{14}C dating (Tjallingii et al., 2010; Bui et al., 2013; Thanh et al., 2021) were recovered from the paleo-Dong Nai River. In contrast, in the paleo-Tien and paleo-Hau rivers, several meters (3–5 m) of thick sand deposits hindered coring. Consequently, the transgressive deposits that filled the incised valleys and formed the Holocene sediment cover across the shelf were primarily recovered along the paleo-Dong Nai River (Figs. 3-5). Correlation of sediment cores clearly demonstrates that the backfilling of the incised valleys had occurred (Tjallingii et al., 2010; Fig. 9), reflecting sea-level rise. In incised valleys along the paleo-Dong Nai and paleo-Hau Rivers, we can identify two sedimentary units representing fluvial (U1.2) and estuarine (U1.3) facies. The sedimentary unit U1.2 was deposited under fluvial conditions and was likely formed during the early transgression from 19.6 to 14.6 ka (Thanh et al., 2021). The oldest ^{14}C age was measured at core 3−68, showing 13.3 ka (Tjallingii et al., 2010; Fig. 9). Cores recovered from the paleo-Dong Nai River penetrating U1.3 were investigated. These sediment characteristics of U1.3 and the seismic facies identified on seismic profiles indicate estuarine facies (Thanh et al., 2021).

The ^{14}C dating ages of estuarine sediments identified within incised valleys indicate that the unit U1.3 was deposited during the late transgression 14.6 to 7.8 ka (Tjallingii et al., 2010; Bui et al., 2013; Thanh et al., 2021, and see Fig. 9).

Unit U1.4 was observed on the entire shelf, generating the Holocene cover of the shelf. The ^{14}C dating results for U1.4 range from 9.3 to 7.2 ka. These results allow us to predict that the sediments of U1.4 had deposited mainly during the transgression 10–7 ka. Investigation of surface sediments on the middle shelf shows that most sediment types are sand. The fraction of mud higher than 10% was identified along the paleo-Dong Nai River, while the fraction of mud is lower than 5% on the rest of the middle shelf, even the southern part near the subaqueous Mekong River Delta (Fig. 10).

Three sedimentary units (U1.2, U1.3, and U1.4) were deposited during the transgression. Although the unit U1.2 has not been dated, we can predict that it was deposited during the early sea-level rise from 19.6 to 14.6 ka. These units are assigned to the transgressive system tract (TST1; Thanh et al., 2021). TST1 was mainly developed during the transgression from 19.6 to 8.0 ka. On the shelf, some reworking of sediments after the transgression stage can lead to younger ages.

Unit 1.5 represents clinoforms of the subaqueous Mekong River Delta that have developed since the onset of the Mekong River Delta ~ 8 ka. The subaqueous Mekong River Delta is younger than 3 ka (Xue et al., 2010; Liu et al., 2017). Most sediments deposited to form U1.5 were sandy mud and mud on the foreset slope; some sandy patches were found on the topset surface (Thanh et al., 2017). The U1.5 was assigned to the highstand systems tract (HST1) (Xue et al., 2010; Bui et al., 2013; Liu et al., 2017). The formation of U2.2 and U1.5 is similar: they formed in the context of relative sea-level fall, although U2.2 formed over a longer period. Within the modern Mekong River Delta, regressive (deltaic) sediments dominate over transgressive deposits. Similarly, on the middle shelf, regressive sediments (U2.2) also predominate over transgressive units (U1.4). Thus, deltaic processes are only facilitated during sea-level fall. Investigations of modern sedimentary processes responsible for the formation of U1.5 and adjacent areas would provide additional scientific basis for predicting the future evolution of the Mekong River Delta in the current context of relative sea-level rise.

5.2. Sediment accumulation rate

In previous studies of the Vietnam shelf, sequence stratigraphic analysis has been integrated with other datasets, including river discharge, shelf morphology, sediment distribution, and sediment accumulation rates (Bui et al., 2019; Thanh et al., 2023, 2026). This integrated approach has been applied to elucidate modern sedimentary processes. In this research, some ^{210}Pb data were also processed to establish sediment accumulation pattern across a wide shelf from the subaqueous Mekong River Delta (inner shelf-U1.5) to the middle shelf (Fig. 17). Generally, the subaqueous delta is separated into three zones: topset, foreset, and bottomset. In this study, the bottomset is not typical and does not develop widely. Many seismic profiles cross the subaqueous delta, but the bottomset is not clearly differentiated from the open middle shelf.

The rollover of clinoforms is defined as the boundary separating the topset from the foreset. Studies of clinoforms indicate that the rollover of the subaqueous Mekong River Delta occurs at water depths of 4–6 m (Figs. 8, 15, and 16) (Nittrouer et al., 2017; Eidam et al., 2017; Liu et al., 2017). The clinoforms extend to a water depth of 20–22 m in front of the Mekong River mouths. Overall, the subaqueous Mekong River Delta is distributed in coastal waters at depths of 0–22 m, which is much shallower

compared to other subaqueous deltas (0–50 or 60 m), such as the Mississippi, Yangtze, Fly, and Ganges-Brahmaputra River Deltas (Nittrouer et al., 2017; Eidam et al., 2017). The rollovers of these subaqueous deltas are generally located at water depths of 12–40 m (Nittrouer et al., 2017; Eidam et al., 2017; Liu et al., 2017).

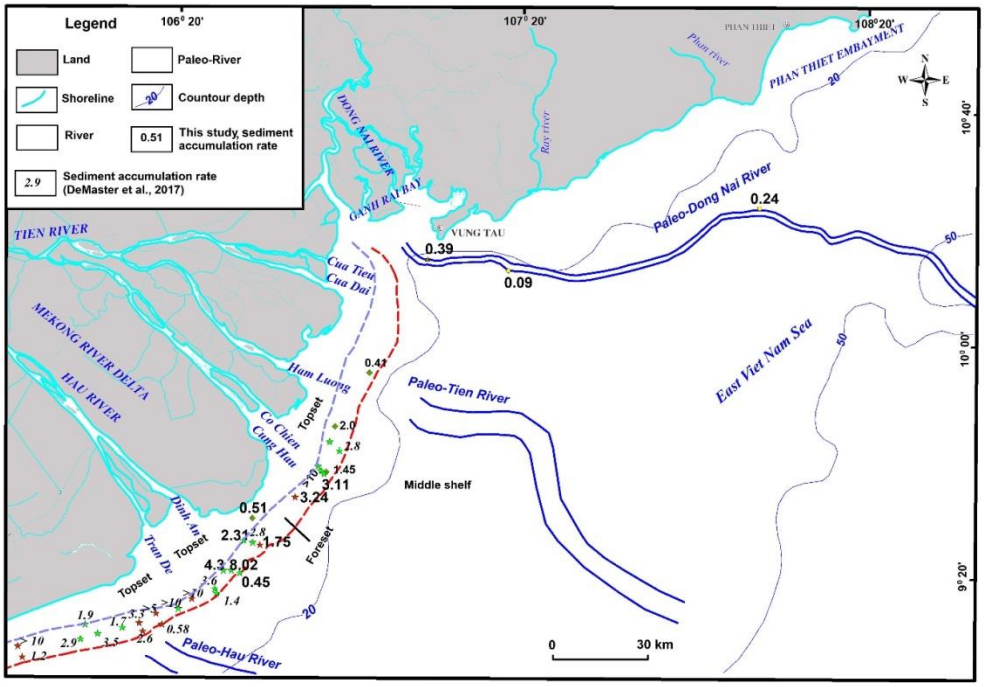

Figure 17. Sediment accumulation rates on the subaqueous Mekong River Delta and adjacent shelf

On the subaqueous Mekong River Delta in front of the Hau River mouths, three transects were carried out. Results show that the sediment accumulation rate at core D17 on the topset is 0.51 cm/y. On the foreset, sediment accumulation rates range from 1 to > 10 cm/y, with higher values on the upper slope and lower values downslope. On the bottomset, the sediment accumulation rate is 0.45 cm/y at core KC11. On the middle adjacent shelf, located more than 20 km from the river mouths, most sediments are sandy with mud content less than 5%, making it unfeasible to measure ^{210}Pb radioactivity. Only one transect was conducted on the middle shelf along the paleo-Dong Nai River, revealing sediment accumulation rates of 0.09–0.39 cm/y (Fig. 11). These results indicate that the middle shelf is a very low-accumulation environment. On this shelf part, most sediments were deposited during the last transgression, and some have been reworked under modern hydrodynamic conditions to form sand waves (Bui et al., 2009; Thanh et al., 2021).

The topset has lower sediment accumulation rates than the foreset due to shallow water depths (2–5 m) that are strongly influenced by waves and currents. In addition, river discharge and tidal outflow interact actively with the shallow topset seabed, further reducing sediment accumulation. During flood seasons, salt-wedge-like stratification occurs on the foreset slope during ebb tide. Meanwhile, high suspended sediment discharge combined with flocculation of fine sediments in saline water results in the greatest sediment accumulation

on the foreset slope. The regulation of sediment accumulation rates on the topset and foreset is consistent with the conceptual model of Walsh et al. (2004). However, the bottomset of the subaqueous Mekong River Delta does not develop typically as in other large deltas. The wide and gently sloping middle shelf is strongly influenced by waves and monsoon-driven currents, which prevent the deposition of fine sediments. Most fine sediments are transported southwestward by the northeast monsoon during winter (Xue et al., 2012, 2014; Liu et al., 2017; Eidam et al., 2017; Thanh et al., 2017; Bui et al., 2009). The transport of fine sediments across the middle shelf during the southwest monsoon in summer has not been documented in previous studies.

Overall, the regulation of sediment accumulation rates can be divided into three zones, from the subaqueous delta to the middle shelf: (i) low rates (< 2 cm/y) on the topset, (ii) high rates on the foreset slope (1– > 10 cm/y) and the rates have a decreasing trend downward foreset slope, and (iii) very low rates on the bottomset to middle shelf (< 0.5 cm/y) (Fig. 18). The patterns of sediment accumulation rates, when considered within a sequence stratigraphic framework, help to further elucidate the developmental trends of sedimentation (Fig. 18).

A comparison between sediment accumulation rates and the present global sea-level rise provides insight into the development of the subaqueous Mekong River Delta under current conditions. Sediment accumulation rates from the bottomset to the middle shelf are generally less than 0.5 cm/y. In contrast, the present global sea-level rise is approximately 0.4 cm/y (Hay et al., 2015) and higher rates in the future due to global warming. These observations indicate that the accommodation space generated by sea-level rise tends to exceed the rate of sediment infilling on the middle shelf.

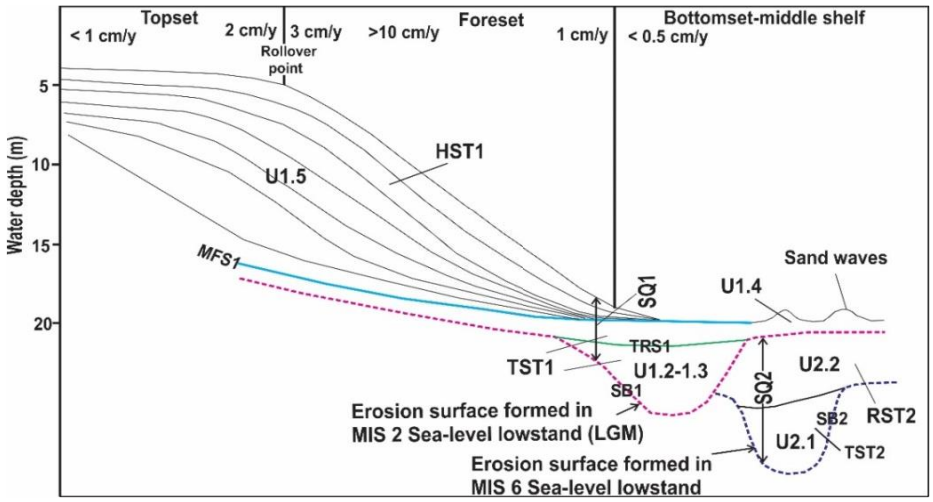

Figure 18. Sediment accumulation rates on the subaqueous delta in front of Mekong River mouths and the middle shelf performed in the Late Quaternary sequence stratigraphic frame

5.3. Sediment transport

Numerous authors have investigated the net sediment transport around the Mekong River Delta and adjacent shelf (Bui et al., 2009; Xue et al., 2012, 2014; Hein et al., 2013; Thanh et al., 2017; Eidam et al., 2017; Liu et al., 2017, Messelhe et al., 2017; Nittrouer et al., 2017; Marchesiello et al., 2019 etc.). These studies indicated a prevailing southwestward sediment transport

toward Ca Mau Cape during the dry season and under the northeast monsoon. In contrast, during the wet season and under the southwest monsoon, sediment transport has mainly been examined within the river estuaries (e.g., Wolanski et al., 1996; Hein et al., 2013; Nowacki et al., 2015; McLachlan et al., 2017; Gugliotta et al., 2017, 2018). Among these works, only Hein et al. (2013) extended their research from the rivers to the middle shelf, showing that suspended sediments in the wet season (high river discharge regime) are dispersed more widely in the east-southeast direction on the shelf, reaching water depths of up to 50 m and extending more than 40 km offshore from the river mouths. However, the role of the southwest monsoon in controlling suspended sediment flux was not suggested in the study of Hein et al. (2013).

Research on shallow surface ocean circulations, in relation to the Mekong River freshwater outflow, indicates that the monthly shallow ocean currents in the southern East Vietnam Sea mainly exhibit two fundamental modes: a clockwise circulation in summer under the influence of the southwest monsoon (June to September), and a counterclockwise circulation in winter under the influence of the northeast monsoon (November to February of the following year). During summer, the clockwise circulation is characterized by northeastward and eastward currents offshore of Vung Tau Cape (Mau et al., 2017). In August and Septemper, Mekong River waters ($S \leq 32$ psu) spread up to about 80 km to 100 km offshore in the northeast direction (Mau et al., 2017). However, the role of east-northeastward and eastward currents offshore of Vung Tau Cape in controlling suspended sediment transport during the southwest monsoon has not been reported in any published articles.

On the other hand, bottom surface sediments collected outside the subaqueous delta, about over 20 km from the Mekong River mouths, consist of sandy sediments with a mud fraction of less than 5% (Fig. 10; Table 1). Sediment stratigraphic studies from this research and previous works (Liu et al., 2017; Thanh et al., 2021) indicate that the Holocene cover (U1.4) on the middle shelf was mainly formed during the postglacial transgression (14.6–8 ka). Sand waves and their directionally migrating patterns observed and described by Bui et al. (2009), and Thanh et al. (2021) are interpreted as the result of transgressive sediment reworking under present-day hydrodynamic conditions. These raise a scientific question: where are suspended sediments deposited, and how are they transported across the shelf during the southwest monsoon?

Results on sediment dynamics from mooring stations on the delta foreset in front of the Hau River mouths during high river discharge show that suspended sediments are transported northward and toward the coast under the southwest monsoon (Eidam et al., 2017). A portion of this suspended sediment can be transported into the Mekong River estuaries and trapped in coastal mangroves during flood tide. Nevertheless, during ebb tide, in combination with high river discharge, suspended sediments can be carried further offshore (Hein et al., 2013) and northward under the influence of the southwest monsoon. As a result, a littoral suspended sediment flux northward along the subaqueous Mekong River Delta can develop during the southwest monsoon season. When this northward flux reaches near the Vung Tau Cape, the local coastal configuration and bathymetry combining with ebb tidal currents can redirect the suspended sediment flux eastward, forming a cross-shelf suspended sediment transport along the paleo-Dong Nai River. This transport may leave a trace along the pathway, which we can identify from surface sediment characteristics on the seabed.

Our results on seabed surface sediments show that the mud fraction is relatively higher along the course of paleo-Dong Nai River

offshore Vung Tau (> 10%) compared to the northern and southern parts of the shelf (< 5%) (Fig. 10). The seabed morphology can be observed partially on the seismic profiles showing a narrow depression (2–3 km in width) along the course of the paleo-Dong Nai River. These findings suggest that a pathway exists for suspended sediment transport along the course of the paleo-Dong Nai River across the shelf during the southwest monsoon (Fig. 10). Nevertheless, the net eastward transport of suspended sediments across the shelf under the southwest monsoon is likely much smaller than the southwestward transport that occurs under the northeast monsoon. Even so, the southwest monsoon continues to transport suspended sediments from the Mekong River eastward into the deep sea.

The combination of sequence stratigraphy analysis, surface sediment distribution, sediment transport, and very low sediment accumulation rates on the middle shelf indicates a limitation in the eastward development of the subaqueous Mekong River Delta toward the middle shelf. As is known, the formation of U2.2 (regression deltaic formation) across the entire shelf requires conditions associated with a long-term sea-level fall. In contrast, global sea levels are rising due to ongoing greenhouse-induced warming (Church and White, 2011; Hay et al., 2015). In addition, sediment discharge from the Mekong River has decreased by more than two-thirds compared to pre-dam conditions (Nowacki et al., 2015; Binh et al., 2020), while subsidence of the delta plain has intensified due to ongoing human activities (Minderhoud et al., 2017; 2018). Therefore, the stratigraphic development regulations in relation to sea-level change and modern sedimentary processes reinforce the conclusion that the subaqueous Mekong River delta has reached its limit of seaward progradation. The Mekong River Delta is gradually retreating in present-day conditions.

6. Conclusions

Sea-level changes are the major force controlling the stratigraphic framework over the last 140 ka, forming two depositional sequences on the northeast shelf off the Mekong River Delta. SQ2 consists of a transgressive systems tract (TST2) that infilled incised valleys during the sea-level rise from the lowstand (MIS 6a) to the highstand (MIS 5e). The TST2 is overlain by a regressive systems tract (RST2) deposited during the subsequent long-term sea-level fall from MIS 5e to MIS 3. SQ1 overlying SQ2 comprises a transgressive systems tract (TST1) and a highstand systems tract (HST1). The TST1 includes fluvial sediments deposited in incised valleys mainly between 19.6 and 14.6 ka, estuarine sediments deposited within incised valleys and adjacent shallow depressions between 14.6 and 7.6 ka, and Holocene marine sediments that blanket the entire shelf, deposited between 10 and 7.2 ka and partially reworked in modern hydrodynamic conditions. The HST1 includes the youngest sedimentary unit representing deltaic deposits formed after 8.0 ka.

Sediment accumulation rates on the subaqueous delta-middle shelf delineate three distinct depositional zones: topset, foreset, and bottomset-middle shelf. The topset is characterized by low accumulation rates of less than 2 cm/y. In contrast, the foreset records the highest rates, ranging from about 1 cm/y to more than 10 cm/y, with an overall tendency to decrease downslope. The bottomset-middle shelf is marked by very low accumulation rates, generally less than 0.5 cm/y. Suspended sediments are transported northward along the subaqueous Mekong River Delta as a littoral flux. They are then deflected eastward near Vung Tau Cape, following the course of the

paleo-Dong Nai River across the shelf under the influence of the southwest monsoon. Cross-shelf suspended transport of suspended sediments during the southwest monsoon is likely much weaker than the southwestward littoral transport during the northeast monsoon.

The predominance of regressive deposits over transgressive deposits within a complete fourth-order (~120 ka) cycle provides evidence for the strong seaward progradation of deltaic sediments during relative sea-level fall. The present relative sea-level rise, reversing the Late Holocene sea-level fall in combination with very low sediment accumulation rates (< 0.5 cm/y) on the delta foreset-middle shelf, suggests that progradation of the subaqueous Mekong River Delta can no longer be sustained. Suspended sediments from the Mekong River during the flood season to the mid-shelf are intensively reworked and transported either landward or farther offshore under tidal and hydrodynamic regimes controlled by monsoonal forcing. As a result, the subaqueous Mekong River Delta is gradually changing from a progradational to a retrogradational state.

Acknowledgments

The authors thank three anonymous reviewers for their comments. We also thank the editorial board for supporting this article. The article is completed under the support of the projects with project codes: NVCC24.03/25-25; VAST05.05/25-26; and UQĐTCB.02/25-27.

References

Binh D.V., Kantoush S., Sumi T., 2020. Changes to long-term discharge and sediment loads in the Vietnamese Mekong Delta caused by upstream dams. Geomorphology, 353, 107011. https://doi.org/10.1016/j.geomorph.2019.107011.

Bui V.D., Schimanski A., Stattegger K., Phach P.V., Tiep N.T., Hai N.T., Thanh N.T., Thanh P.T., 2009. Sandwaves on the Southeast Vietnam shelf recorded by high-resolution seismic profiles: Formation and mechanism. Frontiers of Earth Science, 3, 9–20. https://doi.org/10.1007/s11707-009-0002-z.

Bui V.D., Schimanski A., Stattegger K., Phach P.V., Thanh N.T., 2013. Late Pleistocene-Holocene seismic stratigraphy of the Southeast Vietnam shelf. Global and Planetary Change, 110, 156–169. https://doi.org/10.1016/j.gloplacha.2013.09.010.

Bui V.D., Stattegger K., Kieu N.V., Thanh N.T., Thong B.X., Vu P.N.H., Man H.Q., Trang P.H., 2019. Sediment discharge and storage over the last deglacial highstand period on the central Vietnam shelf off Nha Trang. Geological Quarterly, 63, 395–406. https://doi.org/10.7306/gq.1475.

Carr A.S., Bateman M.D., Roberts D.L., Murray-Wallace C.V., Jacobs Z., Holmes P.J., 2010. The last interglacial sea-level high stand on the southern Cape coastline of South Africa. Quat. Res., 73, 351–363. https://doi.org/10.1016/j.yqres.2009.08.006.

Catuneanu O., Galloway W.E., Kendall C.G., St C., Miall A.D., Posamentier H.W., Strasser A., Tucker M.E., 2011. Sequence Stratigraphy: Methodology and Nomenclature. Newsl. Stratigr, 44(3), 173–245. https://doi.org/10.1127/0078-0421/2011/0011.

Church J.A., White N.J., 2011. Sea-level rise from the Late 19th to the Early 21st Century. Surveys in Geophysics, 32, 585–602. https://doi.org/10.1007/s10712-011-9119-1.

Clark P.U., Dyke A.S., Shakun J.D., Carlson A.E., Clark J., Wohlfarth B., Mitrovica J.X., Hostetler S.W., McCabe A.M., 2009. The Last Glacial Maximum. Science, 325, 710–714. https://doi.org/10.1126/science.1172873.

DeMaster D.J., Liu J.P., Eidam E.F., Nittrouer C.A., Nguyen T.T., 2017. Determining rates of sediment accumulation on the Mekong shelf: Timescales, steady-state assumptions, and radiochemical tracers. Cont. Shelf Res., 147, 182–196. https://doi.org/10.1016/j.csr.2017.06.011.

Eidam E.F., Nittrouer C.A., Ogston A.S., Liu J.P., DeMaster D.V., Nguyen T.T., Nguyen T.N., 2017. Dynamic controls on shallow clinoform geometry: Mekong Delta. Vietnam. Continental Shelf Research, 147, 165–181. https://doi.org/10.1016/j.csr.2017.06.001.

Gugliotta M., Saito Y., Nguyen V.L., Ta T.K.O., Nakashima R., Tamura T., Uehara K., Katsuki K., Yamamoto S., 2017. Process regime, salinity, morphological, and sedimentary trends along the fluvial to marine transition zone of the mixed-energy Mekong River delta. Vietnam. Continental Shelf Research, 147, 7–26. https://doi.org/10.1016/j.csr.2017.03.001.

Gugliotta M., Saito Y., Nguyen V.L., Ta T.K.O., Tamura T., 2018. Sediment distribution and depositional processes along the fluvial to marine transition zone of the Mekong River delta. Vietnam. Sedimentology, 66, 146–164. https://doi.org/10.1111/sed.12489.

Hanebuth T.J.J., Stattegger K., Grootes P.M., 2000. Rapid flooding of the Sunda Shelf: A late-glacial sea-level record. Science, 288, 1033–1035. Doi: 10.1126/science.288.5468.1033.

Hanebuth T.J.J., Stattegger K., Bojanowski A., 2009. Termination of the Last Glacial Maximum sea-level lowstand: The Sunda-Shelf data revisited. Global Planet. Change, 66, 76–84. https://doi.org/10.1016/j.gloplacha.2008.03.011.

Hanebuth T.J.J., Voris H.K., Yokoyama Y., Saito Y., Okuno J., 2011. Formation and fate of sedimentary depocentres on Southeast Asia's Sunda Shelf over the past sea-level cycle and biogeographic implications. Earth Sci. Rev., 104, 92–110. https://doi.org/10.1016/j.earscirev.2010.09.006.

Hay C.C., Morrow E., Kopp R.E., Mitrovica J.X., 2015. Probabilistic reanalysis of twentieth-century sea-level rise. Nature, 517, 481–484. https://doi.org/10.1038/nature14093.

Hein H., Hein B., Pohlmann T., 2013. Recent sediment dynamics in the region of Mekong water influence. Glob Planet Change, 110, 183–194. https://doi.org/10.1016/j.gloplacha.2013.09.008.

Folk R.L., 1954. The distinction between grain size and mineral composition in sedimentary-rock nomenclature. Journal of Geology, 62, 344–359. https://doi.org/10.1086/626171.

Lambeck K., Chappell J., 2001. Sea level change through the Last Glacial Cycle. Science, 292, 679–686. https://doi.org/10.1126/science.1059549.

Liu J.P., DeMaster D.J., Nittrouer C.A., Eidam E.F., Nguyen T.T., 2017. A seismic study of the Mekong subaqueous delta: Proximal versus distal sediment accumulation. Cont. Shelf Res., 147, 197–212. https://doi.org/10.1016/j.csr.2017.07.009.

Masson-Delmotte V., Zhai P., Pirani A., Connors S.L., Péan C., Berger S., Caud N., Chen Y., Goldfarb L., Gomis M.I., Huang M., Leitzell K., Lonnoy E., Matthews J.B.R., Maycock T.K., Waterfield T., Yelekci O., Yu R., Zhou B. (Eds.), 2021. Climate Change 2021: The Physical Science Basis. Contribution of Working Group I to the Sixth Assessment Report of the Intergovernmental Panel on Climate Change. Cambridge University Press. https://www.ipcc.ch/report/ar6/wg1/downloads/report/IPCC_AR6_WGI_SummaryVolume.pdf?.

Marchesiello P., Nguyen N.M., Gratiot N., Loisel H., Anthony E.J., Dinh C.S., Nguyen T., Almar R., Kestenare E., 2019. Erosion of the coastal Mekong delta: Assessing natural against man induced processes. Cont Shelf Res, 181, 72–89. https://doi.org/10.1016/j.csr.2019.05.004.

Matsumoto J., 1997. Seasonal transition of summer rainy season over Indochina and adjacent monsoon region. Advances in Atmospheric Sciences, 14, 231–245. https://doi.org/10.1007/s00376-997-0022-0.

Mau L.D., Cong N.C., Tuan N.V., 2017. Some circulation features during south-west monsoon in southern Vietnam’s waters. Journal of Marine Science and Technology 17(3), 263–270. https://doi.org/10.15625/1859-3097/17/3/10828.

McLachlan R.L., Ogston A.S., Allison M.A., 2017. Implications of tidally-varying bed stress and intermittent estuarine stratification on fine-sediment dynamics through the Mekong's tidal River to estuarine reach. Cont. Shelf Res., 147, 27–37. https://doi.org/10.1016/j.csr.2017.07.014.

Meselhe E., Roelvink D., Wackerman C., Xing F., Thanh V.Q., 2017. Modeling the process response of coastal and deltaic systems to human and global changes: Focus on the Mekong system. Oceanography, 30(3), 84–97. https://doi.org/10.5670/oceanog.2017.317.

Milliman J.D., Farnsworth K.L., 2011. River Discharge to the Coastal Ocean: A Global Synthesis. Cambridge University Press, Cambridge. https://doi.org/10.1017/CBO9780511781247.

Milliman J.D., Meade R.H., 1983. Worldwide delivery of river sediments to the ocean. J. Geol., 91, 1–21.

Milliman J.D., Syvitski J.P.M., 1992. Geomorphic/tectonic control of sediment discharge to the ocean: the importance of small

mountainous rivers. J. Geol., 100, 525–544. https://doi.org/10.1086/629606.

Minderhoud P.S.J., Erkens G., Pham V.H., Bui V.T., Erban L., Kooi H., Stouthamer E., 2017. Impacts of 25 years of groundwater extraction on subsidence in the Mekong delta, Vietnam. Environment Research Letters, 12, 064006. https://doi.org/10.1088/1748-9326/aa7146.

Minderhoud P.S.J., Coumou L., Erbanc L.E., Middelkoopa H., Stouthamera E., Addink E.A., 2018. The relation between land use and subsidence in the Vietnamese Mekong delta. Science of Total Environment, 634(1), 715–726. https://doi.org/10.1016/j.scitotenv.2018.03.372.

Morley C.K., 2012. Late Cretaceous-Early Palaeogene tectonic development of SE Asia. Earth-Science Reviews, 115(1–2), 37–75. https://doi.org/10.1016/j.earscirev.2012.08.002.

Nittrouer C.A., DeMaster D.J., Eidam E.F., Nguyen T.T., Liu J.P., Ogston A.S., and Phung P.V., 2017. The Mekong continental shelf: The primary sink for deltaic sediment particles and their passengers. Oceanography, 30(3), 60–70. https://doi.org/10.5670/oceanog.2017.314.

Nguyen C.T., Schwarzer K., Ricklefs K., 2023. Water-level changes and subsidence rates along the Saigon-Dong Nai River Estuary and the East Sea coastline of the Mekong Delta. Estuar Coast Shelf Sci., 283, 108259. https://doi.org/10.1016/j.ecss.2023.108259.

Nguyen T.T.N., Némery J., Gratiot N., Strady E., Tran V.Q., Nguyen A.T., Aimé J., Peyne A., 2019. Nutrient dynamics and eutrophication assessment in the tropical river system of Saigon - Dongnai (Southern Vietnam). Science of The Total Environment, 653, 370–383. https://doi.org/10.1016/j.scitotenv.2018.10.319.

Nguyen V.L., Ta T.K.O., Saito Y., 2010. Early Holocene initiation of the Mekong River delta, Vietnam, and the response to Holocene sea-level changes detected from DT1 core analyses. Sedimentary Geology, 230, 146–155. https://doi.org/10.1016/j.sedgeo.2010.07.006.

Nowacki D.J., Ogston A.S., Nittrouer C.A., Fricke A.T., Van P.D.T., 2015. Sediment dynamics in the lower Mekong River: transition from tidal River to estuary. J. Geophys. Res. Oceans, 120, 6363–6383. https://doi.org/10.1002/2015JC010754.

Pan T., Murray-Wallace C.V., Dosseto A., Bourman R.P., 2018. The last interglacial (MIS 5e) sea level highstand from a tectonically stable far-field setting, Yorke Peninsula, southern Australia. Mar. Geol., 398, 126–136. https://doi.org/10.1016/j.margeo.2018.01.012.

Posamentier H.W., Allen G.P., 1999. Siliciclastic sequence stratigraphy: concepts and applications. SEPM Concepts in Sedimentology and Paleontology, 7, 210. https://sepm.org/files/brposamentier.ak8vxjen10zkhtzg.pdf.

Quy N.V., Tri T.V., Can N.V., Thang T.T., Ty N.H., Minh N.B., Thien P., Bao N.X., Khuc D.V., Thuc D.D., Toan N.Q., Hoa.T.T., 2007. Geological Map of Viet Nam (Scale 1:1.000.000). Department of Geology and Minerals of Viet Nam, Ministry of Natural Resources and Environments.

Rohling E.J., Fenton M., Jorissen F.J., Bertrand P., Ganssen G., Gaulet J.P., 1998. Magnitude of sea-level lowstands of the past 500000 years. Nature, 394, 162–165. https://doi.org/10.1038/28134.

Schmidt W.J., Hoang B.H., Handschy J.W., Hai V.T., Cuong T.X., Tung N.T., 2019. Tectonic evolution and regional setting of the Cuu Long Basin, Vietnam. Tectonophysics, 757, 36–57. https://doi.org/10.1016/j.tecto.2019.03.001.

Stattegger K., Tjallingii R., Saito Y., Michelli M., Thanh N.T., Wetzel A., 2013. Mid to late Holocene sea-level reconstruction of Southeast Vietnam using beachrock and beach-ridge deposits. Global Planet. Change, 110, 214–222. https://doi.org/10.1016/j.gloplacha.2013.08.014.

Ta T.K.O., Nguyen V.L., Tateishi M., Kobayashi I., Saito Y., Nakamura T., 2002a. Sediment facies and Late Holocene progradation of the Mekong River Delta in Bentre Province, southern Vietnam: an example of evolution from a tide-dominated to a tide- and wave-dominated delta. Sed. Geol., 152, 313–325. https://doi.org/10.1016/S0037-0738(02)00098-2.

Ta T.K.O., Nguyen V.L., Tateishi M., Kobayashi I., Tanabe S., Saito Y., 2002b. Holocene delta evolution and sediment discharge of the Mekong River,

southern Vietnam. Quat. Sci. Rev., 21, 1807–1819. https://doi.org/10.1016/S0277-3791(02)00007-0.

Tanabe S., Saito Y., Lan V.Q., Hanebuth T.J.J., Lan N.Q., Kitamura A., 2006. Holocene evolution of the Song Hong (Red River) delta system, northern Vietnam. Sed. Geol., 187, 29–61. https://doi.org/10.1016/j.sedgeo.2005.12.004.

Thanh N.T., Stattegger K., Unverricht D., Nittrouer C.A., Phach V.P., Liu P., DeMaster D.J., Dung B.V., Anh L.D. Dong M.D., 2017. Surface sediment grain-size distribution and sediment transport in the subaqueous Mekong Delta. Vietnam Journal of Earth Sciences, 39, 193–209. https://doi.org/10.15625/0866-7187/39/3/10266.

Thanh N.T., Cuong D.H., Stattegger K., Bui V.D., Yang S., Chi N.T.K., Tung N.X., Tinh N.V., Nga N.T., 2021. Depositional sequences of the Mekong river delta and adjacent shelf over the past 140 kyr, southern Vietnam. J. Asian Earth Sci., 206, 104634. https://doi.org/10.1016/j.jseaes.2020.104634.

Thanh N.T., Owen M.J., Mackintosh G.K.L., Dung B.V., Stattegger K., Cuong D.H., Andersen Th.J., Tich V.V., Posth N.R., Fruergaard M., Nga N.T., Dung T.T., Hien P.T., 2023. Sequence stratigraphy and sedimentary processes since the last glacial maximum in Nha Phu Bay and adjacent shelf, central Vietnam. Journal of Sea Research, 192, 102352. https://doi.org/10.1016/j.seares.2023.102352.

Thanh N.T., Dung B.V., Diep N.V., Vu P.N.H., Thanh N.C., Khoan D.D., Nga N.T., Hien P.T., Anh L.D., 2026. Post-Last Glacial Maximum seismic stratigraphy and sediment dynamics of the southernmost Central Vietnam shelf. Regional Studies in Marine Science, 96, 104879. https://doi.org/10.1016/j.rsma.2026.104879.

Tjallingii R., Stattegger K., Wetzel A., Phach P.V., 2010. Infilling and flooding of the Mekong River incised valley during deglacial sea-level rise. Quat. Sci. Rev., 29, 1432–1444. https://doi.org/10.1016/j.quascirev.2010.02.022.

Tjallingii R., Stattegger K., Stocchi P., Saito Y., 2014. Rapid flooding of the southern Vietnam shelf during the early to mid-Holocene. J. Quat. Sci., 29, 581–588. https://doi.org/10.1002/jqs.2731.

Unverricht D., Szczuciński W., Stattegger, K., Jagodziński R., Le X.T., Kwong L.L.W., 2013. Modern sedimentation and morphology of the subaqueous Mekong Delta, Southern Vietnam. Global Planet. Change, 110, 223–235. https://doi.org/10.1016/j.gloplacha.2012.12.009.

Vail P.R., 1987. Seismic stratigraphy interpretation procedure. In: Bally, A.W. (Ed), Atlas of Seismic Stratigraphy 27. American Association of Petroleum Geologist Studies in Geology, 1–10. https://sepmstrata.org/page.aspx?&pageid=46&3.

Van Wagoner J.C., Posamentier H.W., Mitchum R.M., Vail P.R., Sarg P.R., Louit J.F., Hardenbol J., 1988. An overview of the fundamental of sequence stratigraphy and key definitions. An Integrated Approach, SEPM Special Publication, 42, 39–45. https://doi.org/10.2110/pec.88.01.0039.

Waelbroeck C., Labeyrie L., Michel E., 2002. Sea level and deep water temperature changes derived from benthonic foraminifera isotopic records. Quat. Sci. Rev., 21, 295–305. https://doi.org/10.1016/S0277-3791(01)00101-9.

Walsh J.P., Nittrouer C.A.,Palinkas C.M., Ogston A.S., Sternberg R.M., Brunskill G.J., 2004 "Clinoform mechanics in the Gulf of Papua, New Guinea", Continental Shelf Research, 24, 2487–2510. https://doi.org/10.1016/j.csr.2004.07.019.

Wolanski E., Ngoc Huan N., Trong Dao L., Huu Nhan N., Ngoc Thuy N., 1996. Fine sediment dynamics in the Mekong River estuary, Vietnam. Estuar. Coast. Shelf Sci., 43(5), 565–582. https://doi.org/10.1006/ecss.1996.0088.

Xue Z., Liu P.J., DeMaster D., Nguyen V.L., Ta T.K.O., 2010. Late Holocene evolution of the Mekong Subaqueous Delta, Southern Vietnam. Marine Geology, 269(1–2), 46–60. https://doi.org/10.1016/j.margeo.2009.12.005.

Xue Z., He R., Liu J.P., Warner J.C., 2012. Modeling transport and deposition of the Mekong River sediment. Continental Shelf Research, 37, 66–78. https://doi.org/10.1016/j.csr.2012.02.010.

Xue Z., Liu J.P., DeMaster D., Leithold E.L., Wan S., Ge Q., Nguyen V.L., Ta T.K.O., 2014. Sedimentary processes on the Mekong subaqueous delta: Clay mineral and geochemical analysis. Journal of Asian Earth Sciences, 79, 520–528. https://doi.org/10.1016/j.jseaes.2012.07.012.